

Direct observation of boron nitride nanocage growth by molecular beam nitridation and liquid-like motion of Fe–B nanoparticles

M. Yeadon,^{*a,b} M. Lin,^{a,c} K. P. Loh,^c C. B. Boothroyd,^a J. Fu^d and Z. Hu^d

^aInstitute of Materials Research and Engineering, 3 Research Link, Singapore 117602.

E-mail: MASYMARK@NUS.EDU.SG; Fax: 65 6872 0785; Tel: 65 6874 8591

^bDepartment of Materials Science, National University of Singapore, Singapore 119260

^cDepartment of Chemistry, National University of Singapore, Singapore 119260

^dLaboratory of Mesoscopic Materials Science and Department of Chemistry, Nanjing University, Nanjing 210093, People's Republic of China

Received 9th June 2003, Accepted 25th July 2003

First published as an Advance Article on the web 27th August 2003

The growth of connected chains of BN nanocages has been achieved by the molecular beam nitridation of nano-sized Fe–B particles. The particles were exposed to ammonia under high vacuum conditions at a temperature of 1000 °C. The experiment was performed in an ultrahigh vacuum chamber built into the column of a high resolution transmission electron microscope enabling direct observation of the process. BN nanocages were observed to form around the Fe–B particles, followed by expulsion of the particles from the cages. Expulsion occurred at a critical shell thickness in a liquid-like manner, despite the experiment being conducted well below the Fe–B liquidus and the particles remained crystalline throughout the experiment. Following expulsion, fresh BN shells formed around the expelled particles, which remained in contact with the previous shell under the influence of surface tension. Chains of connected nanocages were thus formed. The observations provide direct confirmation of the possibility of nanostructure formation by a liquid-like flow of nanocrystalline particles.

Introduction

The growth chemistry and atomic structure of BN nanostructures and thin films have attracted much attention^{1–6} because the wide band gap exhibited by BN suggests interesting applications in novel UV lasers and low-k materials. Following the discovery of the carbon nanotube by Iijima⁷ similar structures have been proposed⁸ and discovered^{1,2} for BN. BN nanotubes have been predicted to display semiconducting properties independent of their chirality^{8,9} together with high ultimate strength and oxidation resistance.

A range of growth techniques have been used for the synthesis of BN nanostructures, including arc discharge,^{2,3} excimer laser irradiation,⁴ low pressure CVD^{5,6} and ball milling followed by annealing at high temperatures^{10,11} using hexagonal BN powder or finely dispersed nickel boride. The growth temperatures and pressures required for these BN syntheses are often high (in the range 1200–1700 °C, at or close to atmospheric pressure). Such temperatures are not readily compatible with microelectronic processing technologies on conventional semiconductor substrates.

The properties and technological applications of BN nanotubes, nanowires and nanospheres have not been fully investigated due to the lack of these materials in sufficient quantity. However, it has been demonstrated for example that BN encapsulated cobalt nanoparticles retain ferromagnetic properties,¹² suggesting that BN nanocages may be useful in protecting magnetic nanoparticles from atmospheric degradation (such as oxidation), and particle sintering.

In this paper we report direct observations of the nucleation and growth of BN nanocages using the heterogeneous reaction between ammonia and iron boride under novel high vacuum conditions. The experiment was performed in the beamline of a JEOL 2000 V ultrahigh vacuum transmission electron microscope (UHV TEM), allowing real-time *in situ* observations of the growth process.

Experimental

FeB nanoparticles were prepared by ball-milling water-free FeCl₃ and NaBH₄ powders (1 : 3.3 mole ratio) for 8 hours, followed by annealing in Ar at 500 °C for 3 hours. Substrates for the experiment were cut from B-doped Si wafers (resistivity 10–15 Ω cm) to dimensions of 6 mm × 2 mm × 0.2 mm in order to facilitate mounting on the sample stage of the electron microscope. The substrates were thinned to perforation in the centre by uniaxial dimpling, followed by chemical etching in a solution of HF : HNO₃ : H₂O 1 : 3 : 1. The nanoparticles were then cast onto the substrates by evaporation from a sonicated ethanol suspension before being loaded into the microscope. The microscope has a base pressure of ~1.5 × 10⁻¹⁰ Torr and is equipped with *in situ* gas injection and solid source deposition capability, together with an electron energy filter for chemical microanalysis.¹³

Results and discussion

TEM observations of the particles revealed excellent size uniformity, and in Fig. 1 we present a bright-field image of a typical area prior to reaction with ammonia. The FeB particles are approximately 10–15 nm in diameter. Electron energy loss spectroscopy (EELS) was performed at this stage and the spectra recorded revealed the presence of the B K-edge and C K-edge, as shown in Fig. 2 (lower trace); no evidence of the presence of nitrogen was observed prior to reaction.

The sample was then heated in the presence of a partial pressure of 5 × 10⁻⁶ Torr NH₃. At ~900 °C, a significant degree of sintering and agglomeration of the FeB nanoparticles was observed. Fluid-like motion of the particle profiles was apparent at and above ~900 °C. The sample was then heated to a maximum temperature of 1000 °C; despite their fluid-like motion, the particles remained crystalline, as determined by the diffraction contrast associated with the particles.

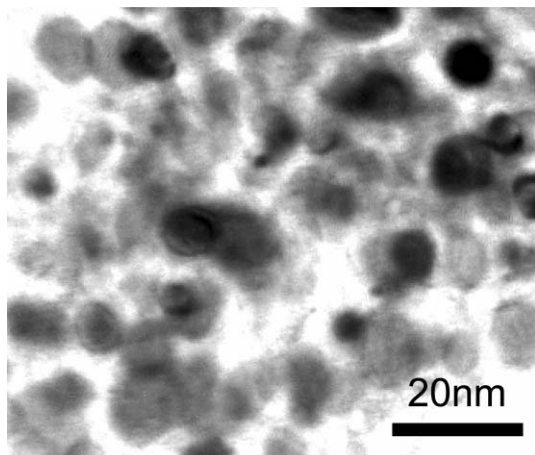


Fig. 1 Bright-field image of the Fe-B nanoparticles prior to heating.

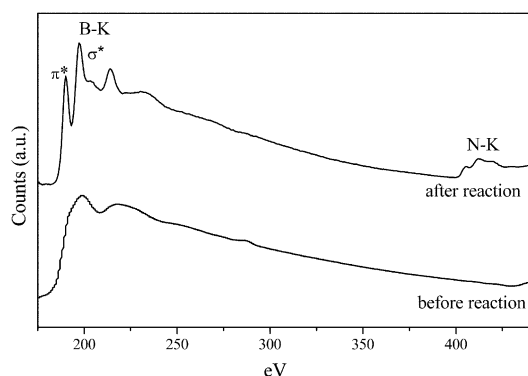


Fig. 2 *In situ* EELS spectra before (lower trace) and after (upper trace) exposure to NH_3 .

After a few minutes exposure to NH_3 at this temperature, the outline of individual particles began to assume a faceted structure, with thin shells being observed to form around the particles. After reaching a certain thickness, approximately 10–15% of the FeB particles were seen to be ejected from the shells that had formed around them, being subsequently located outside the shell but still in contact with it. The process of shell formation took approximately 120 s per shell, with the ejection process taking approximately 1 s. Secondary shells then began to form around the ejected particles. In the case of the particle shown in Fig. 3, the process of cage formation and ejection was repeated four times, before no further ejection events were observed. The particle located at '5' (Fig. 3) was initially located within the BN nanocage at '1'; the series of BN nanocages formed around the particle can be clearly seen, in positions '1'–'5'.

The thickness of the nanocage walls was measured and found to lie in the range ~ 3 – 5 nm. In Fig. 4 we present a high resolution phase contrast image of a representative wall, showing the layered structure of hexagonal BN as viewed along the (0002) planes. The observed lattice spacing corresponds to the expected (0002) spacing of 0.33 nm. The cage shown is still filled with a metallic particle, and a second cage overlapping this cage may be seen in the lower left portion of the image. The presence of occasional defects in the cage walls is apparent. At position 'F', in Fig. 4, a section of the outer shell wall has apparently 'folded' during the initial stages of growth. The feature has some similarities with the observations of Bengu and Marks,¹ who made shape calculations for capped single-walled BN nanostructures that avoid B–B or N–N bonds, which would be unstable, and further investigations of these features are currently in progress. Subsequent growth in this part of the wall has apparently been disturbed, resulting in the

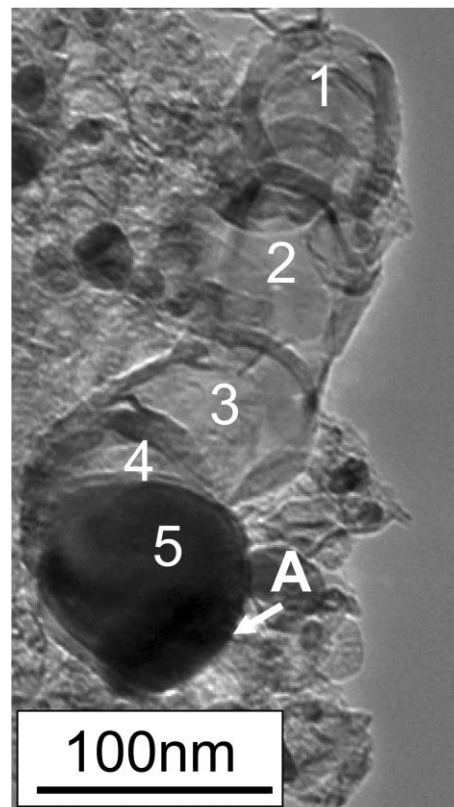


Fig. 3 Bright-field image showing the series of BN nanocages produced by the nanoparticle now contained within shell '5'.

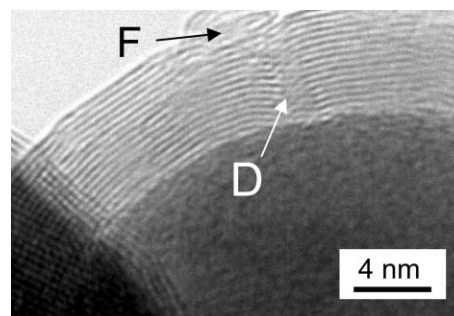


Fig. 4 High-resolution phase contrast image of the BN layer structure. The observed lattice spacing corresponds to the (0002) planes of hexagonal BN, $d_{0002} = 0.333$ nm.

through-thickness defect at 'D' which has propagated through the entire thickness of the wall.

Calculations based on simple mass balance show that the maximum amount of BN that could be produced by a single particle of FeB, initially 80 nm in diameter, is approximately consistent with the amount of BN observed to form in our experiments (Fig. 3). Assuming complete conversion of an 80 nm diameter FeB particle to Fe (*i.e.* complete exhaustion of B), a total of four complete shells, each ~ 3 nm in diameter, could be generated by the complete reaction of elemental boron with the nitrogen species. This would be approximately sufficient to generate the 5 shells observed in Fig. 3, allowing for the sharing of walls between shells.

The details of the ejection process may be seen in the video frames presented in Fig. 5, which were recorded immediately before (Fig. 5(a)) and during (Fig. 5(b)–(d)) the ejection process. Frames (b), (c) and (d) were recorded 360, 400 and 1280 ms after frame (a). From the image in Fig. 5(b), a dynamic contact angle of 150° can be measured between the BN/Fe–B interface and the dewetting Fe–B particle surface.

The equilibrium value of the contact angle θ between a liquid

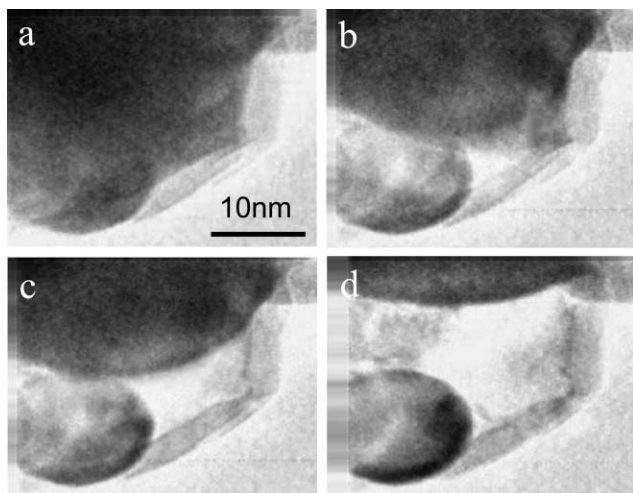


Fig. 5 Video frames captured from the particle expulsion sequence showing the dewetting of the nanoparticle from the BN cage wall. The frames were recorded at (a) $t = 0$ ms, (b) $t = 360$ ms, (c) $t = 400$ ms and (d) $t = 1280$ ms.

and solid defines the wetting behaviour of the liquid, and obeys the classical equation of Young:

$$\cos \theta = \frac{\sigma_{SV} - \sigma_{SL}}{\sigma_{LV}}$$

where σ_{SV} , σ_{SL} and σ_{LV} are the solid/vapour, solid/liquid and liquid/vapour interfacial energies, respectively. Although in our experiments the Fe–B particle remains crystalline, its observed behaviour is liquid-like for the purposes of this equation due to the high mobility of the constituent atoms. A contact angle in excess of 90° implies a non-wetting BN/Fe–B interface. The energy of the interface between FeB and BN is therefore higher than the combined energies of the “liquid-like” FeB/vacuum interface and the BN/vacuum interface. This is consistent with our observations, since no detectable Fe–B remains on the inner walls of the shells following particle expulsion.

EELS spectra were recorded post-nitridation and a representative spectrum is shown in Fig. 2 (upper trace). The spectrum now shows a distinct B K-edge and a N K-edge, with the notable absence of C. The ionization edges π^* and σ^* correspond to the sp^2 hybridization of BN, as expected for the formation of hexagonal BN.

Based on our experimental observations we propose that growth of the BN nanocages proceeds by reaction of nitrogen species at the surface of the FeB particle, with Fe acting as a catalyst for the reaction. The Fe–B phase diagram indicates that FeB is stable to 1650°C .¹⁴ At 1000°C there are no liquid phases expected throughout the entire composition range. As the B content of FeB decreases below 50 atomic% at a temperature of 1000°C , Fe₂B (solid) and FeB are the equilibrium phases (stable to 1389°C), whilst below 33% B, solid Fe and Fe₂B are expected, with a eutectic at 1174°C . The entire experiment is therefore conducted well below the melting temperatures of all expected FeB stoichiometries.

We propose that initial nucleation of BN occurs at the interface between the particle and the support, with the subsequent growth of the BN shell around the particle free surface. A region of uncoated Fe–B surface remains, as may be seen at the leading edge ‘A’ of the particle (arrowed) in Fig. 3. Thermal fluctuation of this leading edge during shell growth is most likely a contributing factor to incomplete shell growth.

Nitrogen-bearing species may be supplied to the particle/shell interface either by diffusion through the shell wall, or by diffusion along the particle/shell interface. Dissolution of nitrogen species in the Fe–B crystal, followed by incorporation

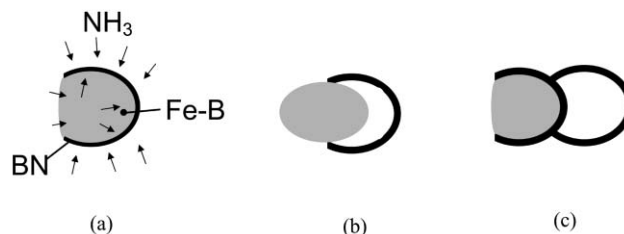


Fig. 6 Schematic diagram of (a) the growth of a BN shell around an Fe–B nanoparticle, followed by (b) strain-induced ejection, and (c) the subsequent formation of a second shell connected to the first.

into the growing shell is also a possibility; these processes are illustrated schematically in Fig. 6(a).

In some cases, high resolution TEM images recorded after cooling to room temperature suggest the presence of metallic species within the cage wall, trapped between BN layers. The presence of the metallic species within the wall would indicate that the metal became incorporated during the growth process, becoming trapped by the overgrowth of further BN layers. This lends further support to our proposal that BN growth is taking place at the particle/shell interface (growth by addition to the inner wall of the shell) rather than at the interface between the shell and the vacuum.

As the thickness of the shell increases, and inward growth continues, the inner diameter of the shell decreases and consequently strain energy will build up in both the BN shell wall and the Fe–B particle. At a critical shell thickness, the strain energy of the system will exceed that required for expulsion of the particle from the cage by dewetting, and the ejection process shown in Fig. 5 will take place. This is illustrated schematically in Fig. 6(b). Provided sufficient B remains within the cage, the formation of a second BN shell around the freshly exposed particle surface, Fig. 6(c), can then occur. We note that the shells remain in fixed positions relative to the substrate throughout the growth sequence, with only migration of the Fe–B particle being observed.

The formation of carbon nanocages and also single-walled nanotubes has been observed by arc-discharge experiments using carbon anodes containing transition metal catalysts.¹⁵ In our experiments, only nanocages are observed to form. The reason for this may be related to the timescales involved in our *in situ* annealing experiments compared with those of arc-discharge synthesis. Prior to nitride formation, we observed the sintering (coarsening) of a significant proportion of the FeB particles, on a timescale of the order of tens of seconds. The formation of nanotubes from these larger, agglomerated nanoparticles will be less favourable than from smaller nanoparticles due to capillary effects, and thus the formation of nanocages was observed to dominate our experiments. In the case of arc-discharge experiments, heating of the carbon/catalyst material to high temperatures occurs on a much shorter timescale (near instantaneous heating), in conditions under which the metal catalyst particles are able to assume and retain diameters of the order of a few nm, as established from *ex situ* TEM experiments. This will be more conducive to nanotube formation.

The low partial pressure of NH₃ during the reaction, yet rapid rate of BN growth, implies a high reaction efficiency between impinging ammonia molecules and boron. Assuming NH₃ supply from the gas phase is the rate limiting step, application of the simple gas law equations suggests that the probability of incorporation of impinging ammonia molecules is ~ 0.1 – 1% . The occasional defects observed in high resolution lattice images of the shell walls (such as ‘D’ in Fig. 4) could act as rapid diffusion paths for the reactive gas species to the Fe–B interface, in addition to diffusion along the particle/shell interface.

The influence of the illuminating electron beam on the

observed shell growth was checked by examining areas of the sample that were not subject to irradiation during growth. In addition, periodic observations of fresh areas of the sample were made during the growth process, with no significant differences between irradiated and non-irradiated areas being observed.

Chen and coworkers^{10,16} have reported observations of bamboo-type BN nanostructures with diameters up to 100 nm, synthesized by annealing ball-milled BN powders at 1300 °C under nitrogen. TEM images showed a continuous endohedral capillary structure with Fe particles trapped within the free ends of the tubes. A growth mechanism involving continuous shape transformations of the Fe particles as they became coated with BN (by solid state diffusion) was suggested. Our observations lend substantial support to this proposed mechanism, since we have demonstrated that liquid-like capillary flow of high melting point material such as Fe–B is possible at temperatures as low as 900 °C. This is 400 °C lower than the temperature at which Chadderton and Chen's experiments were performed. Our experiments thus provide direct evidence of the possibility of liquid-like flow in a broader class of experiments involving fine metal particles at elevated temperatures.

Cathodoluminescence (CL) measurements were performed *ex situ* on samples nitrided for between 10 and 60 minutes under the same experimental conditions. Clear emission peaks were detected, and the data are presented in Fig. 7, obtained at a temperature of 150 K. In each case, emission was centered at ~370 nm, corresponding to an energy of 3.36 eV. The CL signal can be seen to increase substantially with increasing

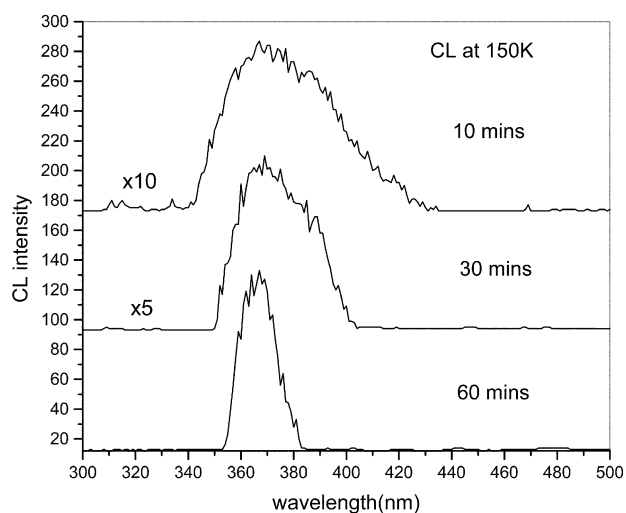


Fig. 7 Cathodoluminescence spectra recorded after 10, 30 and 60 minutes exposure to ammonia.

nitridation time, whilst the FWHM decreases, from ~50 nm after 10 minutes, to ~20 nm after 60 minutes nitridation. The asymmetry of the peak also decreases with nitridation time, as longer wavelength emission is suppressed. This is most likely due to the reduction in mid-gap defects due to surface and related effects as the thickness of the nanocages increases.

Conclusion

In conclusion, we have directly observed the growth of chains of BN nanocages, synthesized by molecular beam nitridation of supported FeB under high vacuum conditions. Multiple nanocages were formed from a single Fe–B particle by a mechanism of strain-induced particle expulsion. The observed liquid-like behaviour at temperatures well below the melting temperature provides direct evidence of the possibility of growth models for related nanostructured materials involving liquid-like flow of metal nanoparticles.

Acknowledgements

The authors acknowledge the Singapore Agency for Science, Technology and Research (ASTAR) and the Ministry of Education (MOE) for supporting this work.

References

- 1 E. Bengu and L. D. Marks, *Phys. Rev. Lett.*, 2001, **86**, 2385–2387.
- 2 N. G. Chopra, R. J. Luyken, K. Cherrey, V. H. Crespi, M. L. Cohen, S. G. Louie and A. Zettl, *Science*, 1995, **269**, 966–967.
- 3 M. Kuno, T. Oku and K. Suganuma, *Diamond Relat. Mater.*, 2001, **10**, 1231–1234.
- 4 D. Golberg, Y. Bando, M. Eremets, K. Takemura, K. Kurashima and H. Yusa, *Appl. Phys. Lett.*, 1996, **69**, 2045–2047.
- 5 O. R. Lourie, C. R. Jones, B. M. Bartlett, P. C. Gibbons, R. S. Ruoff and W. E. Buhro, *Chem. Mater.*, 2000, **12**, 1808–1810.
- 6 K. F. Huo, Z. Hu, F. Chen, J. J. Fu, Y. Chen, B. H. Liu, J. Ding, Z. L. Dong and T. White, *Appl. Phys. Lett.*, 2002, **80**, 3611–3613.
- 7 S. Iijima, *Nature*, 1991, **354**, 56–58.
- 8 A. Rubio, J. L. Corkill and M. L. Cohen, *Phys. Rev. B*, 1994, **49**, 5081–5084.
- 9 X. Blase, A. Rubio, S. G. Louie and M. L. Cohen, *Europhys. Lett.*, 1994, **28**, 335–340.
- 10 L. T. Chadderton and Y. Chen, *J. Crystal Growth*, 2002, **240**, 164–169.
- 11 Y. Chen, J. Fitzgerald, J. S. Williams and S. Bulcock, *Chem. Phys. Lett.*, 1999, **299**, 260–264.
- 12 H. Kitahara, T. Oku, T. Hirano and K. Suganuma, *Diamond Relat. Mater.*, 2001, **10**, 1210–1213.
- 13 R. K. K. Chong, M. Yeadon, W. K. Choi, E. A. Stach and C. B. Boothroyd, *Appl. Phys. Lett.*, 2003, **82**, 1833–1835.
- 14 *Binary Alloy Phase Diagrams*, ed. T. B. Massalski, J. L. Murray, L. H. Bennett and H. Baker, American Society for Metals, Metals Park, OH, 1986.
- 15 S. Seraphin, *J. Electrochem. Soc.*, 1995, **142**, 290–297.
- 16 Y. Chen, L. T. Chadderton, J. Fitzgerald and J. S. Williams, *Appl. Phys. Lett.*, 1999, **74**, 2960–2962.